Wakefield Excitation in Magnetized Quantum Plasma

P. Kumar* and C. Tiwari

Department of Physics, University of Lucknow, Lucknow — 226007, India

Received: 01.02.2023 & Accepted: 26.09.2023

Doi: 10.12693/APhysPolA.144.226 *e-mail: drpunitlko@gmail.com

A study of the wakefield excitation in a magnetized quantum plasma is presented. The high-density plasma has been magnetized through a magnetic field applied in the longitudinal direction. Using a recently developed quantum hydrodynamic model and a perturbative technique, taking into account the quantum effects of Fermi pressure and Bohm potential, electric and magnetic wakefields were obtained for the Gaussian profile of the electromagnetic pulse. Electrons are trapped in the wakefields and accelerated to extremely high energies. It is observed that the quantum effects significantly affect the wakefield excitation. Quantum dispersive effects tend to reduce the acceleration gradient, whereas the external magnetic field helps with self-focusing and also contributes to acceleration. The axial and radial forces acting on a test electron have been calculated.

topics: quantum plasma, wakefields, electron acceleration, quantum hydrodynamic (QHD) model

1. Introduction

In the past two decades, the acceleration of electrons by a laser wakefield [1] has been the focus of scientists throughout the globe, thereby leading to a number of theoretical and experimental investigations. An intense electromagnetic pulse can create a wake of plasma oscillations under the action of ponderomotive force. The electrons are then trapped in the wake and can thus be accelerated to extremely high energies. The pioneering idea of Tajima and Dawson has been theoretically explored and experimentally verified [2–23]. Intense laser beams or bunches of relativistic electrons have been used to excite plasma waves. High electric field strengths (10–100 GV/m) were produced by intense laser beams in the form of bunches of relativistic electrons, thereby opening possibility for compact GeV particle accelerators. Recently, electron acceleration up to the TeV regime has been proposed by plasma wakefield accelerators using protons to drive plasma wakefield driven by electron bunches [24].

The application of magnetic fields significantly influences the laser–plasma interactions since it affects the self-focusing property of the laser beam. As the magnetic field increases, the extent of self-focusing increases, thus a magnetic field enhances the rate of self-focusing. Additionally, in order to avoid phenomena such as electromagnetic filamentation or slipping instability, it is worth to apply a stabilizing external longitudinal magnetic field [25], which not only suppresses instabilities but also gives rise to a large number of new wave branches, thereby substantially expanding the possibilities of the wakefield acceleration scheme. Numerous theoretical and simulation studies [26–37] have been performed on the wakefield excitation in a magnetized plasma. Also experimental studies have been conducted on the wakefields in a magnetized plasma [38].

Recently, studies concerning high-density plasmas (quantum plasma) gained great attention, and pertinent research activities in this area have been observed. Quantum effects appear in ultra-small electronic devices [39], dense astrophysical plasmas [40], ultracold plasmas [41], laser plasmas [42], plasmonics [43], inertial confinement fusion (ICF) [44], laser compression based plasma experiments [45], quantum well [46], quantum free electron lasers (FEL) [47], etc. The quantum plasma has high density, low temperature, and the particles follow the Fermi–Dirac distribution as compared to the classical plasma having low density, high temperature with particles following the Maxwell–Boltzmann distribution.

The study of quantum effects becomes important when the thermal de-Broglie wavelength associated with the charged particle, i.e., $\lambda_{\mathrm{B}}{=}\hbar/(2\pi m\, k_{\mathrm{B}}T)$, approaches the electron Fermi wavelength λ_{F} and exceeds the electron Debye radius λ_{De} (viz., $\lambda_{\mathrm{B}}{\sim}\lambda_{\mathrm{F}} > \lambda_{\mathrm{De}}$). Furthermore, degeneracy and quantum effects play a significant role when the average inter-particle distance ($\sim n_0^{-1/3}$) becomes of the same order or is smaller than λ_{B}, i.e., $n_0\lambda_{\mathrm{B}}^3 \geq 1$. However, other condition for degeneracy is that the thermal temperature (T) of the system must be less than the Fermi temperature (T_{F}) which is related to the equilibrium density (n_0) of the charged particles. In a quantum plasma, electron

degeneracy leads to electron tunneling through the quantum Bohm potential [48–51]. The quantum effects of Fermi statistical pressure and the quantum Bohm force influence the electron dynamics, resulting in collective interactions [48, 52, 53]. Studies concerning the dispersion of nonlinear propagation of waves in quantum plasma have been carried out [54–60]. It has been demonstrated that quantum effects can be important even in the classical regime [61, 62]. The excitation of electrostatic wakefields in a quantum plasma by the ponderomotive force has been studied [63–66] and it has been found that the plasma number density plays an important role in the transition from wakefield generation to soliton formation [67].

In the present paper, a detailed analytical study of the plasma wakefield generation in a magnetized quantum plasma was carried out. The interaction picture was built up using a recently developed quantum hydrodynamic (QHD) model, which consists of a set of equations describing the transport of charge density, momentum (including the Bohm potential), and energy in a charged particle system. The QHD model is a macroscopic model and its application is limited to those systems that are large compared to the Fermi length of the species in the system. The advantage of the QHD model over kinetic descriptions is its numerical efficiency, direct use of the macroscopic variables of interest such as momentum and energy, and the easy way the boundary conditions are implemented. This allows us to study of nonlinear phenomena relatively easier, which is why the QHD approach is preferred for describing such phenomena in quantum plasma [39, 67]. A perturbative technique involving orders of the incident electromagnetic wave have been used to obtain explicit electric and magnetic wakefields. Further, the accelerating force acting on a test electron has been evaluated. The results show that the accelerating force decreases due to the collective effects of statistical pressure and the quantum Bohm force. It is also observed that the energy density of the wakefield is larger as compared to the unmagnetized case. Such a study has not been reported in literature so far.

In Sect. 2, the lowest order fast oscillating plasma electron velocities and density perturbations have been derived. By combining the time-averaged current densities with Maxwell's equations, the generated electric and magnetic wakefields were obtained in Sect. 3. In Sect. 4, the axial and radial forces acting on a moving test electron have been derived and analyzed graphically. Section 5 is devoted to summary and discussion.

2. Electromagnetic wave propagation

We consider the propagation of a linearly polarized *electromagnetic* (e.m.) wave having an electric field $\boldsymbol{E} = \hat{\boldsymbol{e}}_x\, E_o \cos(kz - \omega t)$ ($\hat{\boldsymbol{e}}_x$ is the unit vector of polarization), where E_o, ω, and k are the amplitude, frequency, and wave number of the e.m. wave, respectively, in a uniform magnetized ($\boldsymbol{b} = b\hat{e}_z$) quantum plasma of density n_o. In a quantum plasma, electrons obey the equations [69]

$$\frac{\partial \boldsymbol{v}}{\partial t} = -\frac{e}{\gamma m}\Big[\boldsymbol{E} + \frac{1}{c}(\boldsymbol{v}\times\boldsymbol{B})\Big] - \frac{1}{2}\nabla\big(\boldsymbol{v}\cdot\boldsymbol{v}\big) + \boldsymbol{v}\times\big(\nabla\times\boldsymbol{v}\big) - \frac{v_{\rm F}^2}{3n_o^2\gamma}\frac{\nabla n^3}{n} + \frac{\hbar^2}{2m^2\gamma^2}\nabla\left(\frac{1}{\sqrt{n}}\nabla^2\sqrt{n}\right), \tag{1}$$

$$\frac{\partial n}{\partial t} + \nabla\cdot(n\boldsymbol{v}) = 0, \tag{2}$$

and

$$\nabla\cdot\boldsymbol{E} = -4\pi e\,\big(n - n_o\big), \tag{3}$$

where n ($= n_o + n^{(1)}$) is the electron density, $n^{(1)}$ is the perturbation term, m is the electron rest mass, $\hbar$ is Planck's constant divided by 2π, and $v_{\rm F}$ ($= \sqrt{2k_{\rm B}T_{\rm F}/m}$) is the Fermi velocity. The fourth term on the right-hand side of (1) denotes the force due to the Fermi electron pressure. The Fermi electron pressure for a one-dimensional Fermi gas at zero temperature is given as $P_{\rm F} = mv_{\rm F}^2 n^3/(3n_o^2)$. As we have mentioned in Sect. 1, for degeneracy the thermal temperature must be less than the Fermi temperature, which is possible only at zero temperature, where all electrons have energies below the Fermi temperature [69–71]. It is assumed that the Fermi electron pressure dominates over the electron thermal pressure — the pressure appropriate for a high-density plasma with moderate or low electron temperature. The fifth term of (1) is the quantum Bohm potential and is due to quantum corrections in density fluctuation. The classical equations may be recovered in the limit $\hbar \to 0$. Ions form a neutralizing background in the dense plasma. Perturbatively, expanding (1) and (2) up to the first order of the electromagnetic field, we get

$$\frac{\partial \boldsymbol{v}^{(1)}}{\partial t} = -\frac{e}{\gamma_o m}\boldsymbol{E}^{(1)} - \frac{e}{\gamma_o mc}\Big(\boldsymbol{v}^{(1)}\times\boldsymbol{b}\Big) - \frac{v_{\rm F}^2}{\gamma_o n_o}\nabla n^{(1)} + \frac{\hbar^2}{4m^2\gamma_o^2}\frac{1}{n_o}\nabla\Big(\nabla^2 n^{(1)}\Big), \tag{4}$$

and

$$\frac{\partial n^{(1)}}{\partial t} + \big(n_o\nabla\boldsymbol{v}^{(1)} + \boldsymbol{v}^{(1)}\cdot\nabla n_o\big) = 0, \tag{5}$$

where the subscript "o" signifies the unperturbed quantities and the superscript "(1)" denotes the first order perturbed quantities. Assuming the perturbed density to vary as $n^{(1)} = \eta\exp(\mathrm{i}(kz - \omega t))$ and simultaneously treating (4) and (5), we arrive at

$$\frac{\partial^2 n^{(1)}}{\partial t^2} = \frac{eE_o k n_o}{m}\Big(1 + \frac{\omega_b^2}{\omega^2 - \omega_b^2}\Big)\sin(kz - \omega t) - \frac{eE_o k n_o}{m}\frac{\omega\omega_b}{\omega^2 - \omega_b^2}\cos(kz - \omega t) + n^{(1)}k^2\Big(v_{\rm F}^2 + \frac{\hbar^2 k^2}{4m^2}\Big)\Big(1 - \frac{\omega_b^2 + \omega^2}{\omega^2 - \omega_b^2}\Big), \tag{6}$$

where $\omega_b = \frac{eb}{mc}$ is the cyclotron frequency of the plasma electrons due to an applied external magnetic field in a collisionless quantum plasma. As a solution of (6), we get the first-order perturbed particle density as

$$n^{(1)} = -\frac{ekn_oE_o\Omega_q}{m}\Bigg[\left(1+\frac{\omega_b^2}{\omega^2-\omega_b^2}\right)\sin(kz-\omega t) - \frac{\omega\omega_b}{\omega^2-\omega_b^2}\cos(kz-\omega t)\Bigg], \tag{7}$$

where

$$\Omega_q = \left[\omega^2 + k^2\left(v_{\rm F}^2+\frac{\hbar^2k^2}{4m^2}\right)\left(1-\frac{\omega_b^2+\omega^2}{\omega^2-\omega_b^2}\right)\right]^{-1}. \tag{8}$$

When a high-intensity short e.m. pulse interacts with the magnetized quantum plasma, a ponderomotive force associated with the wave field acts due to which the plasma electrons oscillate with the frequency of the electromagnetic wave. This high-frequency fluctuation in charge density leads to the generation of longitudinal electric field and velocity given, respectively, by

$$E_z^{(1)} = -\omega_{po}^2E_o\Omega_q\Bigg[\left(1+\frac{\omega_b^2}{\omega^2-\omega_b^2}\right)\cos(kz-\omega t) + \frac{\omega\omega_b}{\omega^2-\omega_b^2}\sin(kz-\omega t)\Bigg] \tag{9}$$

and

$$v_z^{(1)} = ac\,\Omega_q\Omega_p\Bigg[-\left(1+\frac{\omega_b^2}{\omega^2-\omega_b^2}\right)\sin(kz-\omega t) + \frac{\omega\omega_b}{\omega^2-\omega_b^2}\cos(kz-\omega t)\Bigg], \tag{10}$$

where $\omega_{po}^2 = 4\pi n_oe^2/m$ is the electron plasma frequency, a $(= \frac{eE_o}{mc\omega})$ is the normalized radiation field amplitude, and $\Omega_p = (\omega_{po}^2 + k^2v_{\rm F}^2 + \frac{\hbar^2k^4}{4m^2})$. The generated field and velocity critically depend on the variation of ω with ω_b and attain a maximum value near the resonance $\omega \approx \omega_b$.

3. Wakefield generation

In order to study the wakefield generation in a magnetized quantum plasma, it is assumed that the e.m. wave does not evolve significantly as it transits a plasma electron [72]. The plasma fluid equations are written in terms of independent variables $\xi = z - ct$ and $\tau = t$. The plasma electron experiences a static e.m. field and hence the field variations with respect to τ are neglected in the plasma fluid equations. In order to obtain the electric and magnetic wakefields, the time-dependent Maxwell's equations are used

$$\nabla\times\boldsymbol{E} = -\frac{1}{c}\frac{\partial\boldsymbol{B}}{\partial t} \tag{11}$$

and

$$\nabla\times\boldsymbol{B} = \frac{4\pi}{c}\boldsymbol{J} + \frac{1}{c}\frac{\partial\boldsymbol{E}}{\partial t}. \tag{12}$$

Assuming the e.m. pulse to have a radial Gaussian profile and the generated fields to be axisymmetric, Maxwell's equations in the cylindrical polar coordinates are

$$\frac{\partial E_r}{\partial\xi} - \frac{\partial E_z}{\partial r} = \frac{\partial B_\theta}{\partial\xi}, \tag{13}$$

$$\frac{\partial E_r}{\partial\xi} - \frac{\partial B_\theta}{\partial\xi} = \frac{4\pi}{c}J_r, \tag{14}$$

$$\frac{\partial E_z}{\partial\xi} = \frac{4\pi}{c}J_z - \frac{1}{r}\frac{\partial(rB_\theta)}{\partial r}, \tag{15}$$

where J_r and J_z are the transverse and axial current densities, respectively. Substituting the first-order quantities in the Lorentz force equation, one gets the lowest (second) order slow components of velocities

$$\frac{\partial v_z}{\partial\xi} = \frac{e}{mc}E_z + \frac{v_{\rm F}^2}{n_oc}\nabla n + \frac{\partial}{\partial\xi}\left\{\frac{ca^2\Omega_q^2\Omega_p^2}{4}\left[\left(1+\frac{\omega_b^2}{\omega^2-\omega_b^2}\right)^2+\frac{\omega_b^2\omega^2}{(\omega^2-\omega_b^2)^2}\right]\right\} \tag{16}$$

and

$$\frac{\partial v_r}{\partial\xi} = \frac{e}{mc}E_r + \frac{v_{\rm F}^2}{n_oc}\nabla n - \frac{rca^2\,\Omega_q^2\Omega_p^2}{r_o^2}\left[\left(1+\frac{\omega_b^2}{\omega^2-\omega_b^2}\right)^2+\frac{\omega_b^2\omega^2}{(\omega^2-\omega_b^2)^2}\right], \tag{17}$$

where E_z and E_r represent the axial and radial electric wakefields. The last term on the right-hand side of (16) is obtained by substituting the value $\left[v_z^{(1)}\right]^2$ averaged over the polar angle θ. In deriving (16) and (17), it is found that the ponderomotive nonlinear effects $\nabla(\boldsymbol{v}\cdot\boldsymbol{v})$ contribute to the transverse as well as longitudinal wakefield generation. However, the nonlinear terms $\boldsymbol{v}\times\boldsymbol{B}$ and $\boldsymbol{v}\times(\nabla\times\boldsymbol{v})$ representing the vortex motion contribute only to the transverse velocity components. Further, the ponderomotive force is modified due to the contribution of the first-order longitudinal velocity of plasma electrons. Combining (15) and (16) gives

$$\left(\frac{\partial^2}{\partial\xi^2}+k_p^2\right)E_z = -\frac{\partial}{\partial\xi}\left(\frac{1}{r}\frac{\partial}{\partial r}(rB_\theta)\right) - \frac{mc^2\Omega_q^2\Omega_p^2k_p^2}{4e}\left[\left(1+\frac{\omega_b^2}{\omega^2-\omega_b^2}\right)^2+\frac{\omega_b^2\omega^2}{(\omega^2-\omega_b^2)^2}\right]\frac{\partial a^2}{\partial\xi}, \tag{18}$$

where $k_p^2 = k_{po}^2\,(1 + n^{(1)}/n_o)$. Combining (13) and (14), and substituting (17) gives

$$E_r = -\frac{1}{k_p^2}\frac{\partial^2E_z}{\partial\xi\partial r} + \frac{mrS\,c^2a^2\Omega_q^2\Omega_p^2}{er_o^2}, \tag{19}$$

where

$$S = \left(1+\frac{\omega_b^2}{\omega^2-\omega_b^2}\right)^2 + \frac{\omega_b^2\omega^2}{(\omega^2-\omega_b^2)^2}. \tag{20}$$

Equations (19) and (20) are the governing equations for the generation of axial and transverse electric wakefields in a dense magnetized quantum plasma. Perturbatively expanding (19) and equating orders, the lowest order axial wakefield is given as

$$\left(\frac{\partial^2}{\partial\xi^2}+k_{po}^2\right)E_z^{(0)} = -\frac{mSc^2k_{po}^2\Omega_q^2\Omega_p^2}{4e}\frac{\partial a^2}{\partial\xi}. \tag{21}$$

Let us assume a Gaussian pulse profile of the form

$$a^2 = a_r^2\sin^2\left(\frac{\pi\xi}{L}\right), \tag{22}$$

where $a_r^2 = a_o^2\exp(-2r^2/r_o^2)$. The energy density of a high-frequency e.m. pulse is assumed to be high enough such that the high-frequency e.m. pulse is changing its shape on a longer timescale, as compared to the wakefield generation process, which is easily achievable for a short pulse [34]. The solutions to (21) for lowest order axial wakefields within ($0 \le \xi \le L$) and behind the e.m. pulse ($\xi < 0$) are, respectively, given by

$$E_z^{(0)} = \tfrac{\varepsilon k_{po}f\,S\Omega_q^2\Omega_p^2}{8}\,\Big[\sin(k_{po}(L-\xi))+\tfrac{k_{po}L}{2\pi}\sin(\tfrac{2\pi\xi}{L})\Big] \tag{23}$$

and

$$E_z^{(0)} = \tfrac{\varepsilon k_{po}f\,S\Omega_q^2\Omega_p^2}{8}\,\Big[\sin(k_{po}\xi)+\sin(k_{po}(L-\xi))\Big], \tag{24}$$

where $\varepsilon{=}mc^2a_r^2/e$ and $f{=}(1{-}k_{po}^2L^2/(4\pi^2))^{-1}$.

Similarly, from (19) the lowest (zeroth) order transverse wakefields within ($0 \le \xi \le L$) and behind ($\xi < 0$) the pulse are, respectively,

$$E_r^{(0)} = -\tfrac{\varepsilon rfS\Omega_q^2\Omega_p^2}{2r_o^2}\Big[\cos\big(k_{po}(L-\xi)\big)-\cos\big(\tfrac{2\pi\xi}{L}\big)\Big] -\tfrac{\varepsilon rS\Omega_q^2\Omega_p^2}{2r_o^2}\Big[\cos\big(\tfrac{2\pi\xi}{L}\big)-1\Big] \tag{25}$$

and

$$E_r^{(0)} = -\tfrac{r\varepsilon fS\Omega_q^2\Omega_p^2}{2r_o^2}\Big[\cos\big(k_{po}(L-\xi)\big)-\cos\big(k_{po}\xi\big)\Big] -\tfrac{r\varepsilon S\Omega_q^2\Omega_p^2}{2r_o^2}\Big[\cos\big(\tfrac{2\pi\xi}{L}\big)-1\Big)\Big]. \tag{26}$$

The lowest order magnetic wakefield within the pulse is $B_\theta^{(0)} = 0$, whereas behind the pulse the field is given by

$$B_\theta^{(0)} = -\tfrac{\Omega_q^2\varepsilon rS\Omega_p^2}{2r_o^2}\left[\cos\left(\tfrac{2\pi\xi}{L}\right)-1\right]. \tag{27}$$

This field is zero on the axis ($r = 0$).

The first-order equation for the axial wakefield is obtained from (18)

$$\left(\frac{\partial^2}{\partial\xi^2}+k_{po}^2\right)E_z^{(1)} = -\frac{\partial}{\partial\xi}\Big(\frac{1}{r}\frac{\partial\big(rB_\theta^{(0)}\big)}{\partial r}\Big)-\frac{n^{(1)}k_{po}^2E_z^{(0)}}{n_o} -\frac{\pi}{L}\frac{mc^2k_{po}^2S\Omega_q^2\Omega_p^2}{4e}\frac{n^{(1)}}{n_o}a_r^2\sin\left(\frac{2\pi\xi}{L}\right). \tag{28}$$

The respective first-order longitudinal wakefields (within the pulse and on the back of the pulse) are obtained by substituting zeroth-order quantities into (28), i.e.,

$$E_z^{(1)} = \tfrac{n'k_{po}\varepsilon fS\Omega_q^2\Omega_p^2}{8}\Big\{\tfrac{k_{po}(L-\xi)}{2}\cos(k_{po}(L-\xi)) +\big(f{+}1\big)\Big[\sin(k_{po}(L-\xi))+\tfrac{k_{po}L}{2\pi}\sin(\tfrac{2\pi\xi}{L})\Big]\Big\} -\tfrac{n'k_{po}\varepsilon fS\Omega_q^2\Omega_p^2}{16}\sin(k_{po}(L-\xi)) \tag{29}$$

and

$$E_z^{(1)} = -\varepsilon fS\Omega_q^2\Omega_p^2\Big\{\tfrac{k_{po}n'}{16}\sin(k_{po}L)\cos(k_{po}\xi) -\tfrac{n'Lk_{po}^2}{16}\Big[\cos(k_{po}(L-\xi))-\cos(k_{po}\xi)\Big] -\tfrac{n'k_{po}}{32}\Big[\sin(k_{po}(2L-\xi))+\sin(k_{po}\xi)\Big] -\left[\tfrac{n'k_{po}}{8}+\tfrac{\left(1-\frac{2r^2}{r_o^2}\right)}{k_{po}r_o^2}\right]\Big[\sin(k_{po}\xi)+\sin(k_{po}(L-\xi))\Big]\Big\}, \tag{30}$$

where $n' = n^{(1)}/n_o$.

The first-order transverse electric wakefields within and at the back of the pulse are obtained, respectively, as

$$E_r^{(1)} = \tfrac{rn'fS\Omega_q^2\Omega_p^2\varepsilon}{2r_o^2k_{po}}\Big\{\tfrac{(L-\xi)k_{po}^2}{2}\sin(k_{po}(L-\xi)) -k_{po}(1{+}f)\Big[\cos(k_{po}(L-\xi))-\cos(\tfrac{2\pi\xi}{L})\Big]\Big\} +\tfrac{\varepsilon S\Omega_q^2\Omega_p^2r}{r_o^2}\sin^2(\tfrac{\pi\xi}{L}) \tag{31}$$

and

$$E_r^{(1)} = -\tfrac{rS\Omega_q^2\varepsilon f\Omega_p^2}{r_o^2}\Big\{-\tfrac{n'}{4}\sin(k_{po}L)\sin(k_{po}\xi) -\tfrac{k_{po}n'L}{4}\Big[\sin(k_{po}(L-\xi))+\sin(k_{po}\xi)\Big] +\left[\tfrac{n'}{2}+\tfrac{8(1-\frac{r^2}{r_o^2})}{k_{po}^2r_o^2}\right]\Big[\cos(k_{po}(L-\xi))-\cos(k_{po}\xi)\Big]\Big\} +\tfrac{mrSc^2a_r^2\Omega_p^2\Omega_q^2}{er_o^2}\sin^2(\tfrac{\pi\xi}{L}). \tag{32}$$

The expressions for the first-order magnetic weakfields within and behind the pulse are, respectively,

$$B_\theta^{(1)} = -\tfrac{r\varepsilon n'fS\Omega_q^2\Omega_p^2}{2r_o^2}\Big[\cos(k_{po}(L-\xi))-\cos(k_{po}L)\Big] +\tfrac{\varepsilon rS\Omega_q^2\Omega_p^2}{2r_o^2}(1-n'f)\Big(1-\cos(\tfrac{2\pi\xi}{L})\Big) \tag{33}$$

and

$$B_\theta^{(1)} = \tfrac{r\varepsilon k_{po}n'fLS\Omega_q^2\Omega_p^2}{2r_o^2}\Big[\sin(k_{po}(L-\xi))+\sin(k_{po}\xi)\Big] +\tfrac{\varepsilon rS\Omega_q^2\Omega_p^2}{2r_o^2}\Big(1-\cos(\tfrac{2\pi\xi}{L})\Big). \tag{34}$$

4. Electron acceleration

The maximum axial wakefields within and behind the e.m. pulse in the limit $L \to \lambda_p$ are obtained (by using L' Hospital's rule) as

$$E_{zm} = E_{zm}^{(0)} + E_{zm}^{(1)} = \tfrac{\pi\varepsilon S\Omega_q^2\Omega_p^2}{4}\Big[-\tfrac{\pi}{L}(1+\tfrac{5n'}{4})(1-\tfrac{\xi}{L})\cos(\tfrac{2\pi\xi}{L}) -\tfrac{1}{2L}\Big(1+n'\pi^2(1-\tfrac{\xi}{L})^2+\tfrac{5n'}{4}\Big)\sin(\tfrac{2\pi\xi}{L})\Big] \quad (0 \le \xi \le L), \tag{35}$$

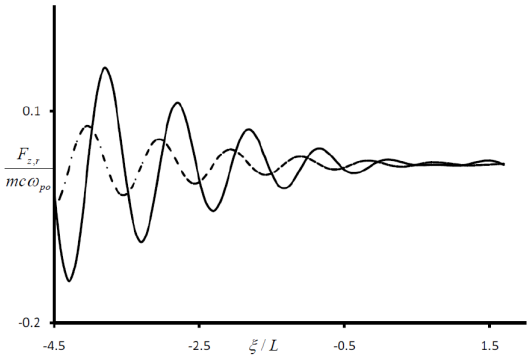

Fig. 1. Variation of the normalized axial $F_z/(mc\omega_{po})$ (solid line) and transverse $F_r/(mc\omega_{po})$ (dashed line) forces acting on a test electron within the pulse with $\frac{\xi}{L}$ (x-axis) for $a_o^2 = 0.9$, $\lambda_p = 15.0$ μm, $r_o = 15.0$ μm, $r = 4.0$ μm, and $\omega_b/\omega = 0.5$.

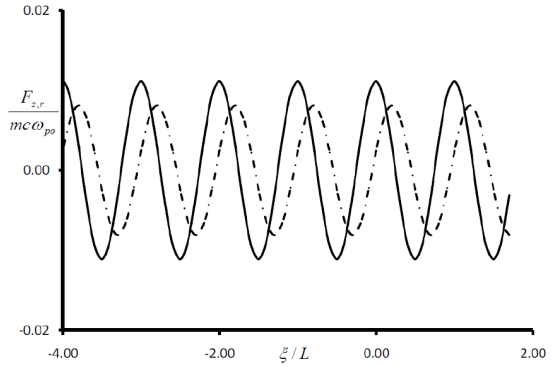

Fig. 2. Variation of the normalized axial $F_z/(mc\omega_{po})$ (dashed line) and transverse $F_r/(mc\omega_{po})$ (solid line) forces acting on a test electron behind the pulse with $\frac{\xi}{L}$ (x-axis) for $a_o^2 = 0.9$, $\lambda_p = 15.0$ μm, $r_o = 15.0$ μm, $r = 4.0$ μm, and $\omega_b/\omega = 0.5$.

$$E_{zm} = -\frac{\varepsilon S\Omega_q^2\Omega_p^2\pi^3 n'}{4L}\sin(\tfrac{2\pi\xi}{L}) - \frac{\varepsilon S\Omega_q^2\Omega_p^2\pi^2}{4L}\left[1+n'+\frac{2L^2}{r_o^2\pi^2}(1-\frac{2r^2}{r_o^2})\right]\cos(\tfrac{2\pi\xi}{L}), \quad (\xi<0). \tag{36}$$

The maximum transverse electric wakefields are given by

$$E_{rm} = E_{rm}^{(0)} + E_{rm}^{(1)} = \frac{\varepsilon rS\Omega_q^2\Omega_p^2}{r_o^2}\frac{\pi\xi}{L}\sin(\tfrac{2\pi\xi}{L}) + \frac{\varepsilon rS\Omega_q^2\Omega_p^2}{2r_o^2}\left[\pi(1-\tfrac{\xi}{L})\sin(\tfrac{2\pi\xi}{L}) - \cos(\tfrac{2\pi\xi}{L})+1\right] + \frac{\varepsilon rn'S\Omega_q^2\Omega_p^2}{32\pi r_o^2}\left[-8\pi^3(1-\tfrac{\xi}{L})^2\cos(\tfrac{2\pi\xi}{L}) + 12\pi^2(1-\tfrac{\xi}{L})\sin(\tfrac{2\pi\xi}{L}) + 8\pi^2(-\tfrac{3\xi}{L}+2\pi)\sin(\tfrac{2\pi\xi}{L})\right], \quad (0\le\xi\le L) \tag{37}$$

$$E_{rm} = \frac{\varepsilon rS\Omega_q^2\Omega_p^2}{2r_o^2}\left[\pi\sin(\tfrac{2\pi\xi}{L}) - \cos(\tfrac{2\pi\xi}{L})+1\right] + \frac{\varepsilon rLS\Omega_q^2\Omega_p^2}{2r_o^2}\left[\left(\frac{g\pi}{2L}+\frac{4L}{\pi r_o^2}\left(1-\frac{r^2}{r_o^2}\right)\right)\sin(\tfrac{2\pi\xi}{L}) - \frac{2\pi^2 g}{L}\cos(\tfrac{2\pi\xi}{L})\right] + \frac{mrSc^2a_r^2\Omega_q^2\Omega_p^2}{er_o^2}\sin(\tfrac{2\pi\xi}{L}), \quad (\xi<0), \tag{38}$$

and the maximum magnetic wakefields are given as

$$B_{\theta m} = -\frac{\pi r\varepsilon S\Omega_q^2\Omega_p^2}{r_o^2}\left(\frac{n'}{2}(1-\tfrac{\xi}{L})-\frac{\xi}{L}\right)\sin(\tfrac{2\pi\xi}{L}), \quad (0\le\xi\le L), \tag{39}$$

$$B_{\theta m} = \frac{\varepsilon rS\Omega_q^2\Omega_p^2}{2r_o^2}\left(1-\cos(\tfrac{2\pi\xi}{L})\right) + \frac{\varepsilon rS\Omega_q^2\Omega_p^2}{r_o^2}\left(n'\pi^2+\tfrac{1}{2}\right)\sin(\tfrac{2\pi\xi}{L}), \quad (\xi<0). \tag{40}$$

The maximum longitudinal force acting on a test electron is $F_z = -eE_{zm}$, and the electron will only be accelerated if $F_z > 0$. The maximum transverse force F_r $(= -eE_{rm}+eB_{\theta m})$ should be $F_r < 0$ to focus the electron towards the axis. In a high-density quantum plasma, near the critical density, the group velocity of the electromagnetic wave approaches zero, and the pump depletion and dephasing lengths become shorter than the plasma wavelength. Consequently, the interaction primarily occurs within one plasma wavelength, and the wave significantly couples to the bulk motion of the plasma [72].

While performing numerical analysis, we consider the astrophysical plasma parameters, i.e., plasma density 10^{26}–10^{29} cm^{-3} and magnetic field strength 10^9–10^{11} Gauss. For a magnetic field of 10^{10} Gauss and a plasma density $n_o = 10^{26}$ cm^{-3}, the value of ω_b comes out to be 1.4×10^{17} s^{-1}, while ω_p will be 1.1×10^{18} s^{-1}, thereby satisfying $\omega_b<\omega_p$. Such a regime is prevalent in neutron stars, magnetars and white dwarfs [73–80]. The present theory is also applicable to semiconductor quantum plasmas, solid density plasmas, compressed plasmas, inertial confinement fusion experiments and to quantum nanowires [81–88] for their respective parameters.

Variations of the normalized axial $F_z/(mc\omega_{po})$ and transverse $F_r/(mc\omega_{po})$ forces acting on a test electron within the e.m. pulse for $a_o^2 = 0.9$, $\lambda_p = 15.0$ μm, $r_o = 15.0$ μm, $r = 4.0$ μm, $\omega_b/\omega = 0.5$ have been shown in Fig. 1. The axial force is greater and leads in phase to the transverse force. Figure 2 depicts the variation of the normalized axial and transverse forces acting behind the e.m. pulse for similar parameters as in Fig. 1. It is seen that behind the pulse, the transverse force is greater than the force in the longitudinal direction.

A plot of the accelerating force with the normalized frequency of the externally applied magnetic field (denoting the strength of the applied magnetic field) has been shown in Fig. 3. The force increases with the applied magnetic field and a rapid increase is observed for $\omega_b/\omega > 0.8$. The force becomes

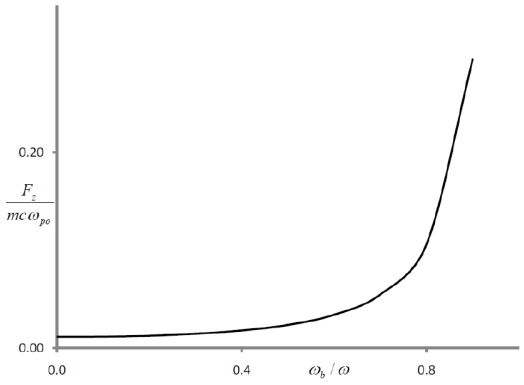

Fig. 3. Variation of the normalized axial force $F_z/(mc\omega_{po})$ with normalized frequency ω_b/ω (x-axis) of the external magnetic field for $a_o^2 = 0.9$, $\lambda_p = 15.0$ μm, $r_o = 15.0$ μm, $r = 4.0$ μm, and $\xi/L = 4.0$.

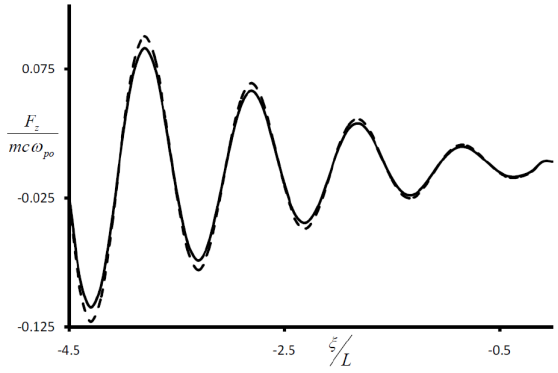

Fig. 4. Variation of the normalized axial force $F_z/(mc\omega_{po})$ acting on an electron within the pulse with $\frac{\xi}{L}$ for a quantum plasma (solid line) and for the classical case in the limit $\hbar \to 0$ (dashed line).

maximal near the resonance, i.e., when $\omega_b \to \omega$. At the resonance $\omega_b = \omega$, the accelerating gradient approaches infinity and the theory breaks down. Thus, optimum gain is obtained near resonance.

The variation of the axial force ($F_z/(mc\omega_{po})$) acting within the pulse has been shown in Fig. 4 for similar parameters as used in Fig. 1. The solid line denotes the variation under the influence of quantum effects, while the dashed line shows the force in the absence of quantum effects in the limit $\hbar \to 0$. It is observed that the force is reduced in quantum plasma by about 10% compared to the classical case. This reduction is due to quantum diffraction effects.

5. Conclusions

We have studied in detail the wakefield generation by an intense electromagnetic pulse traveling through a magnetized quantum plasma. We have used the electron continuity and momentum equations, incorporating quantum statistical pressure and quantum Bohm force, together with the Poisson equation to obtain the perturbed density and velocity. The electric and magnetic wakefields have been derived with the help of the time-dependent Maxwell's equations using a quasi-static approximation for the radial Gaussian field amplitude. It is found that ponderomotive nonlinear effects, quantum force, and quantum statistical pressure contribute to the transverse as well as longitudinal wakefield generation. However, the nonlinear terms representing the vortex motion contribute only to the transverse velocity components. The zeroth- and first-order electric and magnetic wakefields (both transverse and longitudinal) within and behind the pulse have been obtained for a sinusoidal pulse profile. The energy density of the wakefield in the present case is larger by a factor of ω_b^2/ω_{po}^2 compared to the unmagnetized case. The magnification is directly attributed to the additional electromagnetic part of the wakefield.

The maximum axial and transverse forces acting on a test electron due to the wakefields have been evaluated. The variation of these forces with ξ/L has been studied. It is found that even weak, short pulses are capable of generating considerable wakefields. The force behind the pulse is greater than within the pulse. Wakefields generated within the pulse are of the same order, whereas behind the pulse, the axial field is greater than transverse field. Simultaneous acceleration focusing is observed in the regime where $F_z > 0$ and $F_r < 0$. Quantum effects suppress perturbation of the electron number densities and the electric field of the e.m. wakefields. In other words, quantum effects weaken the wakefields and the accelerating field of wakefields. It is found that quantum effects reduce the accelerating force by about 10%, which is due to quantum dispersive effects and may be considered as a classical manifestation of quantum decoherence. This is due to the additional effective pressure created in the plasmas by quantum fluctuations. The additional pressure leads to a more dispersive plasma wave, which weakens the wakefields. On the other hand, the applied magnetic field increases the accelerating gradient, whose effect is much greater than quantum effects, and the optimum acceleration can be achieved by exploiting resonance. The optimum electron acceleration is obtained near resonance. Excited electrostatic wakefields can trap electrons and accelerate them to high energies in the nanoscales in dense plasmas, such as those in compact astrophysical objects like in white dwarf stars, neutron stars, magnetars, etc. The present theory will be also applicable to thin metal films, in the next generation intense laser–solid density plasma experiments, in quantum nanowires, and can also contribute to the development of ultrasmall wakefield accelerators.

Acknowledgments

The authors are grateful to U.G.C., India, for providing assistance through research award scheme.

References

[1] T. Tajima, J.M. Dawson, *Phys. Rev. Lett.* **43**, 267 (1979).

[2] N.E. Aandreev, L.M. Gorbunov, V.I. Kirsonov, A.A. Pegosova, *JETP Lett.* **60**, 713 (1994).

[3] V.A. Balakirev, V.I. Karas, V.I. Levchenko, *Laser Part. Beams* **19**, 597 (2001).

[4] J. Faure, Y. Glinec, A. Pukhov, S. Kiselev, S. Gordienko, E. Lefebvre, J.P. Rousseau, F. Burgy, V. Malka, *Nature* **431**, 541 (2004).

[5] C.G.R. Geddes, C. Toth, J.V. Tilborg, E.Esarey, C.B. Schroeder, D. Bruhwiler, C. Nieter, J. Cary, W.P. Leemans, *Nature* **431**, 538 (2004).

[6] L.M. Gorbunov, P. Mora, A.A. Solodov, *Phys. Plasmas* **10**, 1124 (2003).

[7] K.V. Lotov, *Laser Part. Beams* **26**, 225 (2001).

[8] M.J.H. Luttikhof, A.G. Khachatryan, F.A.V. Goor, K.J. Boller, P. Mora, *Laser Part. Beams* **27**, 69 (2009).

[9] S.P.D. Mangles, C.D. Murphy, Z. Najmudin et al., *Nature* **431**, 535 (2004).

[10] J.R. Marquès, J.P. Geindre, F. Amiranoff, P. Audebert, J.C. Gauthier, A. Antonetti, G.Grillon, *Phys. Rev.Lett.* **76**, 3566 (1996).

[11] K.T. Phuoc, S. Corde, R. Fitour et al., *Phys.Plasmas* **15**, 073106 (2008).

[12] A. Pukhov, J.M.T. Vehn, *Appl. Phys.B: Lasers Opt.* **74**, 355 (2002).

[13] H.P. Schlenvoigt, K. Haupt, A. Debus et al., *Nature Phys.* **4**, 130 (2008).

[14] S.V. Bulanov et. al., *J. Plasma Phys.* **82**, 905820308 (2016).

[15] M.M.A. Elwahab, H.A.E. Elshaikh, Q.M. Yassin, *Open J. App. Sci.* **11**, 354 (2021).

[16] Y. Golian, D. Dorranian, *J. Th. App. Phys.* **11**, 27 (2017).

[17] Y. Golian, M. Aslaninejad, D. Dorranian, *Phys. Plasmas* **23**, 013109 (2016).

[18] J.T. Mendonca, J. Viera, C. William, R. Fedele, *Front. Phys.* **10**, 995379 (2022).

[19] J. Zhu, P. Ji, *Phys. Rev. E* **81**, 036406 (2010).

[20] A. Golovanon, I. Yu. Kastyukov, A. Pukhov, V. Malka, *Phys. Rev. Lett.* **130**, 105001 (2023).

[21] A. Mehdi-Varaki, *Nuc. Inst. Meth. Res. A* **1048**, 168010 (2023).

[22] M. Arfnia, M. Ghorbanalilu, A.R. Niknam, *Phys. Plasmas* **29**, 072305 (2022).

[23] B. Hidding et. al., *Photonics* **10**, 99 (2023).

[24] A. Caldwell, K. Lotov, A. Pukhov, F. Simon, *Nature Phys.* **5**, 363 (2009).

[25] A.T. Amatuni, E.V. Sekhposyan, A.G. Khachatryan, S.S. Elbakian, *Phys. Rep.* **21**, 945 (1995).

[26] G. Brodin, J. Lundberg, *Phys. Rev. E* **57**, 7041 (1998).

[27] A. Holkundkar, G. Brodin, M. Marklund, *Phys. Rev. E* **84**, 036409 (2011).

[28] R.S. Bonati, M.E. Abari, *Phys. Plasmas* **17**, 032101 (2010).

[29] D.N. Gupta, H. Suk, M.S. Hur, *App. Phys. Lett.* **91**, 211101 (2007).

[30] P. Jha, A. Saroch, R.K. Mishra, A.K. Upadhyay, *Phys. Rev. Acc. Beams* **15**, 081301 (2012).

[31] M.S. Hur, D.N.Gupta, H. Suk, *Phys. Lett. A* **372**, 2684 (2008).

[32] J. Vieira, S.F. Martins, V.B. Pathak, R.A. Fonseca, W.B. Mori, L.O. Silva, *Phys. Rev. Lett.* **106**, 225001 (2011).

[33] X.P. Xia, B. Xu, L. Wang, *Optik* **127**, 658 (2016).

[34] P.K. Shukla, G. Brodin, M. Marklund, L. Stenflo, *Phys. Lett. A* **33**, 3165 (2009).

[35] P.K. Shukla, *Physica Scripta* **52**, 73 (1994).

[36] D.A. Burton, A. Noble, *New J. Phys.* **20**, 033022 (2018).

[37] B. Nikrah, S. Jafari, *Iran J. Sci.* **47(2)**, 014426 (2023).

[38] T. Hosokai, A. Zhidkov, A. Yamazaki, Y. Mizuta, M. Uesaka, R. Kodama, *App. Phys. Lett.* **96**, 121501 (2010).

[39] P.A. Markowich, C. Ringhofer, C. Schmeiser, *Semiconductor Equations'*, Vienna, Springer (1990).

[40] Y .D. Jung, *Phys. Plasmas* **8**, 3842 (2001).

[41] W. Li, P.J. Tanner, T.F. Gallagher, *Phys. Rev. Lett.* **94**, 173001 (2005).

[42] D. Kremp, *Phys. Rev. E* **60**, 4725 (1999).

[43] M. Marklund,G.Brodin, L. Stenflo, C.S. Liu, *Euro Phys. Lett.* **84**, 17006 (2008).

[44] M. Borghesi, A. Schiavi, D.H. Campbell et al., *Plasma Phys. Control Fusion* **43**, A267 (2001).

[45] P.K. Shukla, B. Eliasson, *Phys. Rev. Lett.* **99**, 096401 (2007).

[46] G. Manfredi, P.A. Hervieux, *Appl. Phys. Lett.* **91**, 061108 (2007).

[47] A. Serbeto, J.T. Mendonça, K.H. Tsui, R. Bonifacio, *Phys. Plasmas* **15**, 013110 (2008).

[48] C.L. Gardner,C. Ringhofer, *Phys. Rev. E* **53**, 157 (1996).

[49] G. Manfredi, *Fields Inst.Comm.* **46**, 263 (2005).

[50] A. Bret, *Phys. Plasmas***11,** 084503 (2007).

[51] S.V. Vladimirov, Y.O. Tyshetskiy, *Physics-Uspekhi* **54**, 1243 (2011).

[52] G. Manfredi, F. Haas, *Phys. Rev. B* **64**, 075316 (2001).

[53] P.K. Shukla, *Phys. Lett. A* **352**, 242 (2006).

[54] P. Kumar, C. Tewari, *J. Phys.: Conf. Ser.* **208**, 012051(2010).

[55] J.H. Liang, T.X. Hu, D. Wu, Z.M. Sheng, *Phys. Rev. E* **103**, 033207 (2021).

[56] S. Roy, D. Chatterjee, A.P. Misra, *Phys. Scripta* **95**, 015603 (2019).

[57] A.P. Misra, G. Brodin, M. Marklund, P.K. Shukla, *Phys. Plasmas* **17**, 122306 (2010).

[58] M. Stefan, G. Brodin, *Phys. Plasmas* **20**, 012114 (2013).

[59] A. Hussain, M. Stefan, G. Brodin, *Phys. Plasmas* **21**, 032104 (2014).

[60] B. Eliasson, P.K. Shukla, *Phys. Rev. E* **83**, 046407 (2011).

[61] M. Opher et al., *Phys. Plasmas* **8**, 2454 (2001).

[62] G. Brodin, M. Marklund, G. Manfredi, *Phys. Rev. Lett.* **100**, 175001 (2008).

[63] G. Brodin, A. Holkundkar, M. Marklund, *J. Plasma Phys.* **79**, 377 (2013).

[64] P. Kumar, C. Tewari, *Laser Part. Beams* **30**, 267 (2012).

[65] A.R. Holkundkar, G. Brodin, *Phys. Rev. E* **97**, 043204 (2018).

[66] P.K. Shukla, *J. Plasma Phys.* **75(1)**, 15 (2009).

[67] P.K. Shukla, S. Ali, L. Stenflo, M. Marklund, *Phys. Plasmas* **13**, 11211 (2006).

[68] B. Ghosh, S. Chandra, S.N. Paul, *Pramana: Journal of Physics* **78**, 779 (2012).

[69] G. Manfredi, F. Haas, *Phys. Rev. B* **64**, 075316 (2001).

[70] E. Esarey, P. Sprangle, J. Krall, A. Ting, *IEEE J. Quantum Elec.* **33**, 1879 (1997).

[71] A. Atteya et al., *J. Taibah Univ. Sci.* **14(1)**, 1182 (2020).

[72] T. Tajima, X.Q. Yan, T. Ebisuzaki, *Rev. of Mod. Phys.* **4**, 7 (2020).

[73] S.A. Allkhateeb et al., *J. Taibah Univ. Sci.* **17(1)**, 2187606 (2023).

[74] S. Hussain, S. Mahmood, A. Mushtaq, *Astrophys. Space Sci.* **346**, 359 (2013).

[75] W.M. Moslem et al., *Phys. Plasmas* **14**, 082308 (2007).

[76] B. Sahu, A. Sinha, R. Roychoudhury, *Phys. Plasmas* **26**, 072119 (2019).

[77] P.K. Shukla, B. Eliasson, *Rev. Mod. Phys.* **83**, 885 (2011).

[78] D.A. Uzdensky, S. Rightley, *Rep. Prog. Phys.* **77**, 036902 (2014).

[79] M. Marklund, P.K. Shukla, *Rev. Mod. Phys.* **78**, 591 (2006).

[80] S. Ali, W.M. Maslam, P.K. Shukla, R. Schlickeiser, *Phys. Plasmas.* **14**, 082307 (2007).

[81] F. Haas, B. Eliasson, *Phys. Scripta* **90(8)**, 088005 (2015).

[82] A.K. Harding, D. Lai, *Rep. Prog. Phys.* **69**, 2631 (2006).

[83] J. Zhu, P. Ji, *Pl. Phys. Control. Fusion* **54**, 065004 (2012).

[84] Y. Wang, P.K. Shukla, B. Eliassion, *Phys. Plasmas* **20**, 013103 (2013).

[85] S.M. Khorashadizadeh, S. Majedi, A.R. Niknam, *The Euro. Phys. J. Plus* **133**, 77 (2018).

[86] F. Calvayrac, P.G. Reinhard, E. Suraud, C. Ulrich, *Phys. Rep.* **337**, 493 (2000).

[87] J.H. Luscombe, A.M. Bouchard, M. Luban, *Phys. Rev. B* **46**, 10262 (1992).

[88] S. Ali and Ioannis Kourakis, *Emerging Developments and Applications of Low Temperature Plasma*, Chapter – 1, IGI Global (2022).